A Diagnostic Coastal Circulation Model with Application to Conception Bay, Newfoundland

BRAD DE YOUNG, RICHARD J. GREATBATCH, AND KENNETH B. FORWARD

Department of Physics, Memorial University of Newfoundland, St. John's, Newfoundland, Canada

(Manuscript received 7 March 1992, in final form 5 January 1993)

ABSTRACT

A diagnostic circulation model is developed for application to coastal regions. The three-dimensional velocity field can be calculated from a specified density field and wind-stress distribution provided transport is given on boundaries where f/H contours enter the model domain (here f is the Coriolis parameter and H is the ocean depth). The model is an extension of that of Mellor. It includes the effect of vertical mixing and bottom friction and avoids explicit calculation of the JEBAR (joint effect of baroclinicity and relief) term, which can be noisy when a realistic density field is combined with realistic topography. The model can also be used in regions of closed f/H contours. An application of the model to Conception Bay, Newfoundland, illustrates the ease of calculation and yields comparisons with the more classical technique of dynamic height analysis.

1. Introduction

Historically, there has been much effort applied to the problem of indirectly determining ocean currents from measured ocean properties. Indeed, the development of modern oceanography can be traced to the "Scandinavian school" and the development of dynamic height calculations for inferring velocities (Sandström and Helland-Hansen 1903). However, the method suffers from a number of limitations, particularly in regions of variable bottom topography. In this paper, we shall develop and test a numerical model that can easily be applied to density data to infer a consistent velocity field, no matter what the nature of the bottom topography.

The basic approach at the heart of the dynamic method comes from assuming that the flow is geostrophic and hydrostatic. The thermal wind equations can then be used to calculate the velocity field so long as the velocity is known at some reference depth. Often, a level of no motion is assumed and the velocities are calculated relative to this depth. Clearly, problems arise if the ocean is shallower than the depth of the assumed level of no motion. A number of methods have been suggested for getting around this problem. The first, due to Helland-Hansen (1934), involves extending isopycnals horizontally under the bottom of the ocean from their point of intersection with the slope. This ensures that the geostrophic velocity at the bottom is zero if the level of no motion is deeper than the depth of the ocean bottom. It follows that the approach is formally equivalent to the methods of Montgomery (1941) and Csanady (1979) since these take the assumption of zero bottom geostrophic velocity as their starting point. Montgomery (1941) argued that this was reasonable by pointing out that bottom friction will tend to keep the bottom velocities small compared with those above. Csanady (1979), on the other hand, used the assumption of no alongshore variations to force the bottom stress to be zero. If this is parameterized in terms of bottom geostrophic velocity, it follows that this too must be zero. An alternative method is to extend isopycnals along their last observed slopes. This method, which is wrongly attributed to Montgomery (1941) by both Reid and Mantyla (1976) and Tabata et al. (1986), appears to have been introduced by Sverdrup et al. (1942) and later modified by Groen (1948).

Both of the extrapolation techniques just described run into difficulties in regions of irregular bottom topography. For example, where there is a ridge, the density field on each side of the ridge may not match, making extrapolation difficult. Also, the method suffers from the fundamental difficulty that a level of no motion does not, in general, exist in the ocean. Indeed, in many regions flow has been observed to be in the same direction at all depths with near-bottom velocities being a significant fraction of those above. An example is provided by Schmitz (1980) for the recirculation region of the Gulf Stream and, more recently, by Lazier and Wright (1993) for the Labrador Current system. In addition, the restriction of these methods to geostrophy is clearly limiting, especially in shallow regions where vertical mixing, bottom friction, and wind stress are likely to be important. One solution to these problems

Corresponding author address: Dr. Brad de Young, Department of Physics, Memorial University of Newfoundland, St. John's, Newfoundland, Canada A1B 3X7.

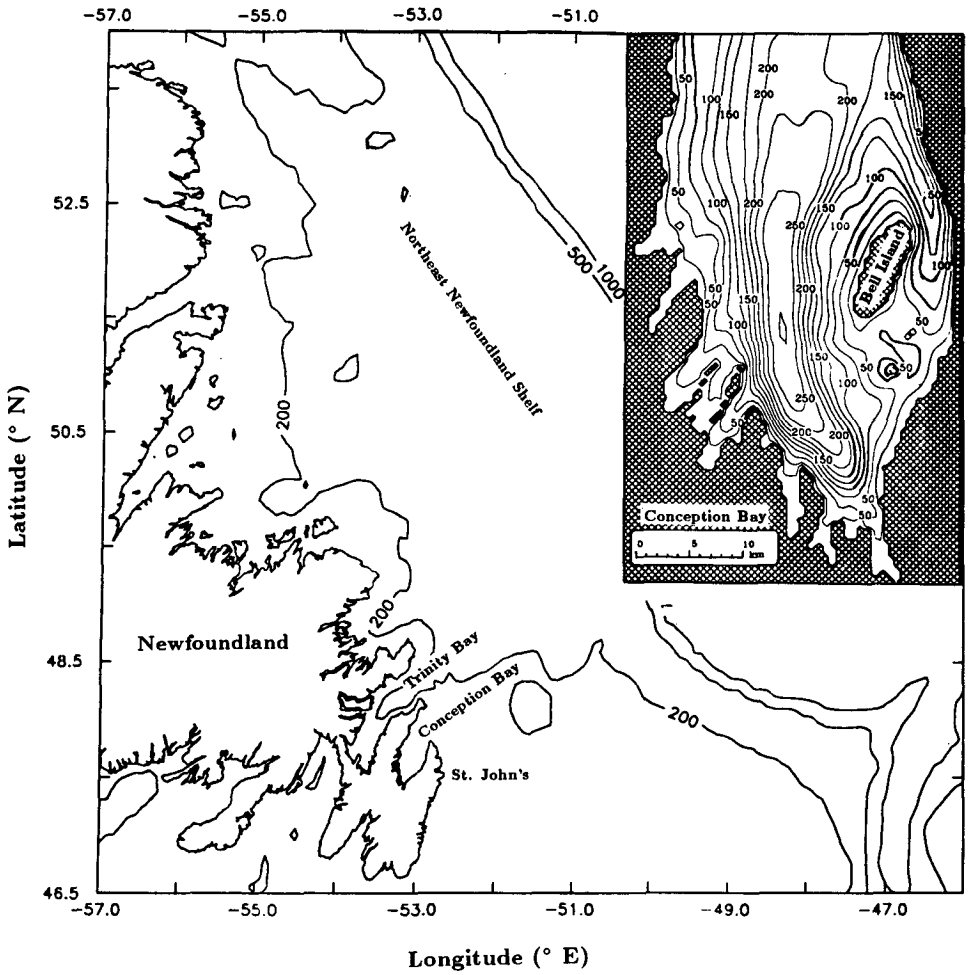

FIG. 1. The bottom topography of the northeast Newfoundland Shelf showing the location of Conception Bay. Depth contours are in meters. The model domain at a resolution of 0.5 km is shown in the panel. The scale in the panel applies to the model domain.

is to use a diagnostic model that solves the equations of motion with these effects included. An early example is provided by the work of Holland and Hirschman (1972), who ran the numerical model of Bryan (1969) with the density field prescribed from an analysis of data collected in the North Atlantic [in fact the forerunner of Levitus (1982)]. A problem with calculations of this kind is that the JEBAR term (the joint effect of baroclinicity and relief) is often very noisy. To get around this, Rattray (1982) suggested working with bottom pressure rather than a volume transport streamfunction. On the other hand, Mellor et al. (1982) replaced the volume transport streamfunction by a new variable such that on an f plane the JEBAR term is completely absorbed and is never explicitly calculated. These authors describe an application of their method to the North Atlantic circulation. Kantha et al. (1982) used the same method to perform a diagnostic calculation of the circulation in the South Atlantic Bight. The model can include the effect of wind stress but does not include vertical mixing or bottom friction [although Herring and Kantha (1990) introduced these effects by using the model iteratively]. Also because the model integrates along f/H contours, where f is the Coriolis parameter and H is the depth of the ocean, it cannot deal with regions where these contours are closed. This is also a problem with Rattray's (1982) model.

The model to be described in this paper is an extension of that of Mellor et al. (1982). It takes advantage of their change of variable to deal with the JEBAR term but includes the effect of vertical mixing, bottom friction, and surface wind stress and can also deal with regions of closed f/H contours. It can be applied in any coastal region and requires only knowledge of the density field, bottom topography, and wind stress and also the vertically integrated transport where f/H contours enter the model domain. Its principal limitations are that the bottom stress must be expressed in terms of bottom geostrophic velocity (Csanady 1982) and

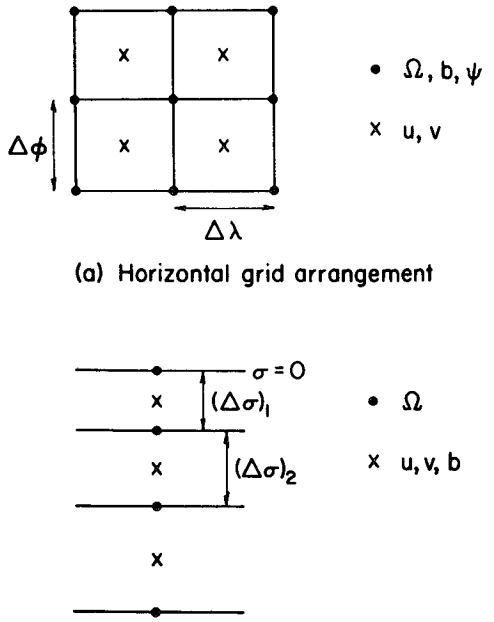

FIG. 2. The Arakawa B-grid arrangement used in the model. Variables are defined in section 2 of the text.

also that it cannot be applied in regions where either f or the density field exhibit large variations (this is discussed at the end of section 2). This means that although the model is suitable for use in shelf regions such as the Newfoundland/Labrador Shelf, it is not suitable for a diagnostic calculation of the entire North Atlantic circulation. In this paper, we describe its application to Conception Bay, Newfoundland, using density data collected as part of the Cold Ocean Productivity Experiment [a description of the physical oceanographic data collected as part of this project can be found in deYoung and Sanderson (1992)]. Current meter data are used to provide the boundary condition at the mouth of the bay and data from the interior are compared with the model results.

Aside from the work of Mellor et al. (1982) and Rattray (1982), another diagnostic coastal circulation model that should be mentioned is that of Lynch et al. (1992). Rather than use a volume transport streamfunction, as we have done here, this model infers the barotropic component of the flow by using a finite-element method to solve for sea level. The restriction to steady state is relaxed by solving the equations in frequency space.

The plan of this paper is as follows. Section 2 describes the model and section 3 the method of solution. The data from Conception Bay are described in section 4 and the application of the model using these data in section 5. Section 6 provides a summary and discussion.

2. The model

The model to be described is diagnostic in that it calculates the 3D velocity field from a specified density field and wind-stress distribution. It is an extension of the model of Mellor et al. (1982) and Kantha et al. (1982) to include the effect of bottom friction. The latter is parameterized in terms of the bottom geostrophic velocity (Csanady 1982). As is well known, the JEBAR term (Sarkisyan and Ivanov 1971) can be very noisy in calculations that combine a realistic density field with realistic bathymetry (Mellor et al. 1982; Rattray 1982). To avoid this problem, a new variable is defined in place of the volume transport streamfunction in such a way that the JEBAR term is completely absorbed and never explicitly calculated. This is the principal advantage of the method. We assume steady flow and neglect the local time derivative and nonlinear advection terms from the momentum equations. The appropriateness of these assumptions for the case of Conception Bay is discussed in section 4.

The model uses coordinates (x, y, σ), where x is measured across the bay, y along it, and $\sigma = z/H$, where $H(x, y)$ is the depth of water and z is measured vertically upwards with $z = 0$ at the sea surface and $z = -H$ at the bottom. In these coordinates, the governing equations are

$$-fv = -\frac{1}{\rho_o}\frac{\partial p}{\partial x} - b\sigma\frac{\partial H}{\partial x} + \frac{1}{H^2}\frac{\partial}{\partial \sigma}\left(\nu\frac{\partial u}{\partial \sigma}\right) \quad (1)$$

$$fu = -\frac{1}{\rho_o}\frac{\partial p}{\partial y} - b\sigma\frac{\partial H}{\partial y} + \frac{1}{H^2}\frac{\partial}{\partial \sigma}\left(\nu\frac{\partial v}{\partial \sigma}\right) \quad (2)$$

$$0 = -\frac{\partial P}{\partial \sigma} - \rho_o bH \quad (3)$$

$$\frac{\partial}{\partial x}(uH) + \frac{\partial}{\partial y}(vH) + \frac{\partial}{\partial \sigma}(\Omega H) = 0, \quad (4)$$

where

$$\Omega = \frac{1}{H}\left[w - \sigma\left(u\frac{\partial H}{\partial x} + v\frac{\partial H}{\partial y}\right)\right] \quad (5)$$

and

$$b = \frac{g}{\rho_o}(\rho - \rho_r). \quad (6)$$

Here u, v, w, and Ω are the velocities in the x, y, z, and σ directions, p is the perturbation pressure, ρ_o is a representative density for seawater, ν is the vertical eddy viscosity, g is the acceleration due to gravity, ρ is the density, b is the negative of the buoyancy, and ρ_r is the horizontally averaged density at each depth z. The Coriolis parameter f is assumed to be a uniform constant, as is clearly reasonable for a bay the size of Conception Bay. It should be noted that because we are using σ as the vertical coordinate, the horizontal pressure gradient

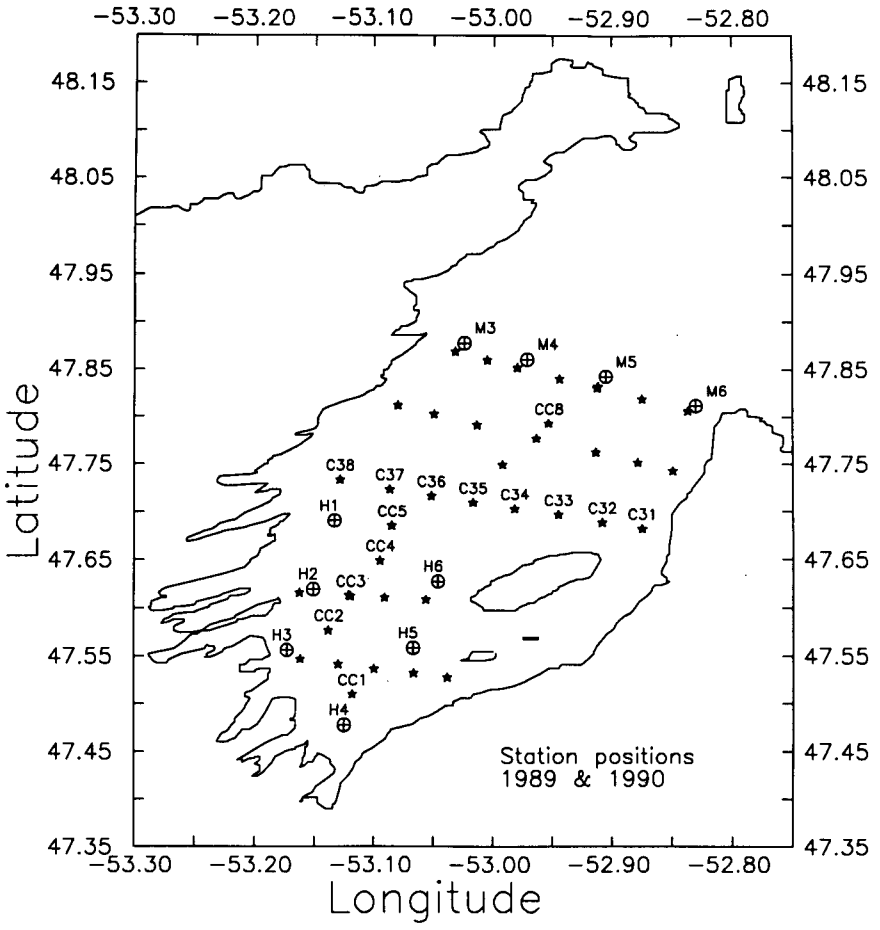

FIG. 3. The CTD stations, indicated with solid stars, used to compile the density data. Mooring locations are indicated with crossed circles. The 1989 moorings are given the designation M (near the mouth) and the 1990 moorings H (near the head).

terms in (1) and (2) appear as the difference between two terms. Because these terms can be large compared to their difference (e.g., Haney 1991), significant error can result. This is why we use b rather than ρ in the hydrostatic equation (3). By subtracting off the horizontally averaged density, the error is significantly reduced. We shall discuss this point further in sections 3 and 5.

At the sea surface ($\sigma = 0$) and bottom ($\sigma = -1$) we have the following boundary conditions. At both $\sigma = 0$ and -1,

$$\Omega = 0. \tag{7}$$

At $\sigma = 0$,

$$\frac{1}{H}\nu\left(\frac{\partial u}{\partial \sigma}, \frac{\partial v}{\partial \sigma}\right) = \frac{1}{\rho_o}(\tau_s^x, \tau_s^y), \tag{8}$$

and at $\sigma = -1$,

$$\frac{1}{H}\nu\left(\frac{\partial u}{\partial \sigma}, \frac{\partial v}{\partial \sigma}\right) = \frac{1}{\rho_o}(\tau_b^x, \tau_b^y). \tag{9}$$

Here (7) is the kinematic condition. In (8) and (9), (τ_s^x, τ_s^y) is the surface wind stress and (τ_b^x, τ_b^y) is the bottom stress. A linear parameterization is used for the latter in terms of bottom geostrophic velocity (u_{gb}, v_{gb}), that is,

$$\tau_b = (\tau_b^x, \tau_b^y) = \rho_o r(u_{gb}, v_{gb}). \tag{10}$$

It should be noted that for the method of solution to work, the bottom friction can be any linear function of (u_{gb}, v_{gb}). In particular, the direction of τ_b can be rotated through some angle from that of (u_{gb}, v_{gb}) [see Csanady (1982)]. For simplicity and given the limitations already inherent in our model, we shall not consider this effect here.

The problem that must be overcome by an inverse model is how to calculate the barotropic component of the flow. To see how this is done we first vertically integrate (1) and (2) to obtain, using (8) and (9),

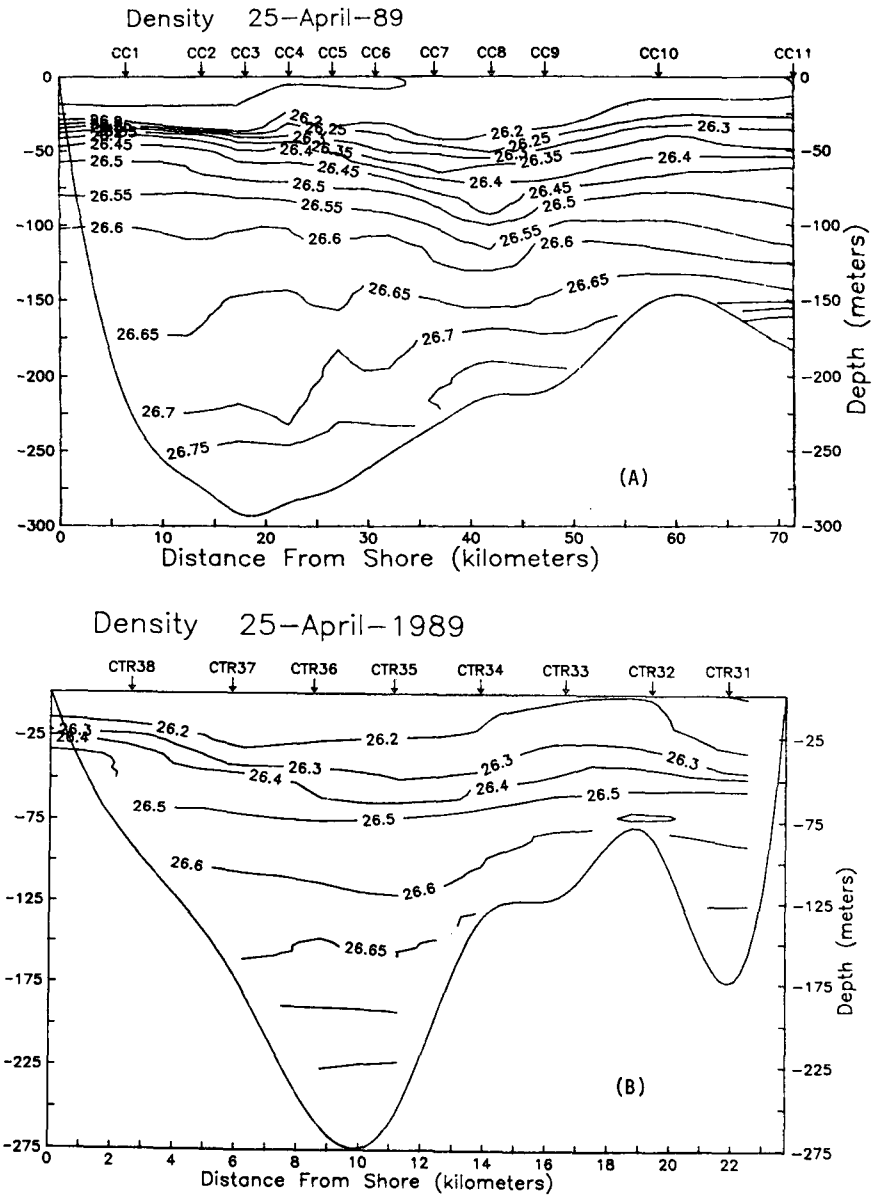

FIG. 4. (a) Density (sigma t) along the axis of the bay, 25 April 1989.
(b) Density (sigma t) across the bay, 25 April 1989. Station locations are shown in Fig. 3.

$$-f\bar{v} = -\frac{1}{\rho_o}\left\{\frac{\partial}{\partial x}\int_{-1}^{o} p d\sigma + \rho_o \frac{\partial H}{\partial x}\int_{-1}^{o} b\sigma d\sigma\right\} + \frac{1}{\rho_o H}(\tau_s^x - \tau_b^x) \quad (11)$$

$$f\bar{u} = -\frac{1}{\rho_o}\left\{\frac{\partial}{\partial y}\int_{-1}^{o} p d\sigma + \rho_o \frac{\partial H}{\partial y}\int_{-1}^{o} b\sigma d\sigma\right\} + \frac{1}{\rho_o H}(\tau_s^y - \tau_b^y), \quad (12)$$

where

$$(\bar{u}, \bar{v}) = \int_{-1}^{o} (u, v) d\sigma. \quad (13)$$

Also, vertically integrating (4) and using (7) enables us to define a volume transport streamfunction with

$$\bar{u}H = -\psi_y, \quad \bar{v}H = \psi_x. \quad (14)$$

Taking $\partial/\partial x$ of (12) minus $\partial/\partial y$ of (11) now gives

$$J\left(\psi, \frac{f}{H}\right) = \frac{1}{\rho_o}\left\{\frac{\partial}{\partial x}\left(\frac{\tau_s^y - \tau_b^y}{H}\right) - \frac{\partial}{\partial y}\left(\frac{\tau_s^x - \tau_b^x}{H}\right)\right\} + \text{JEBAR}, \quad (15)$$

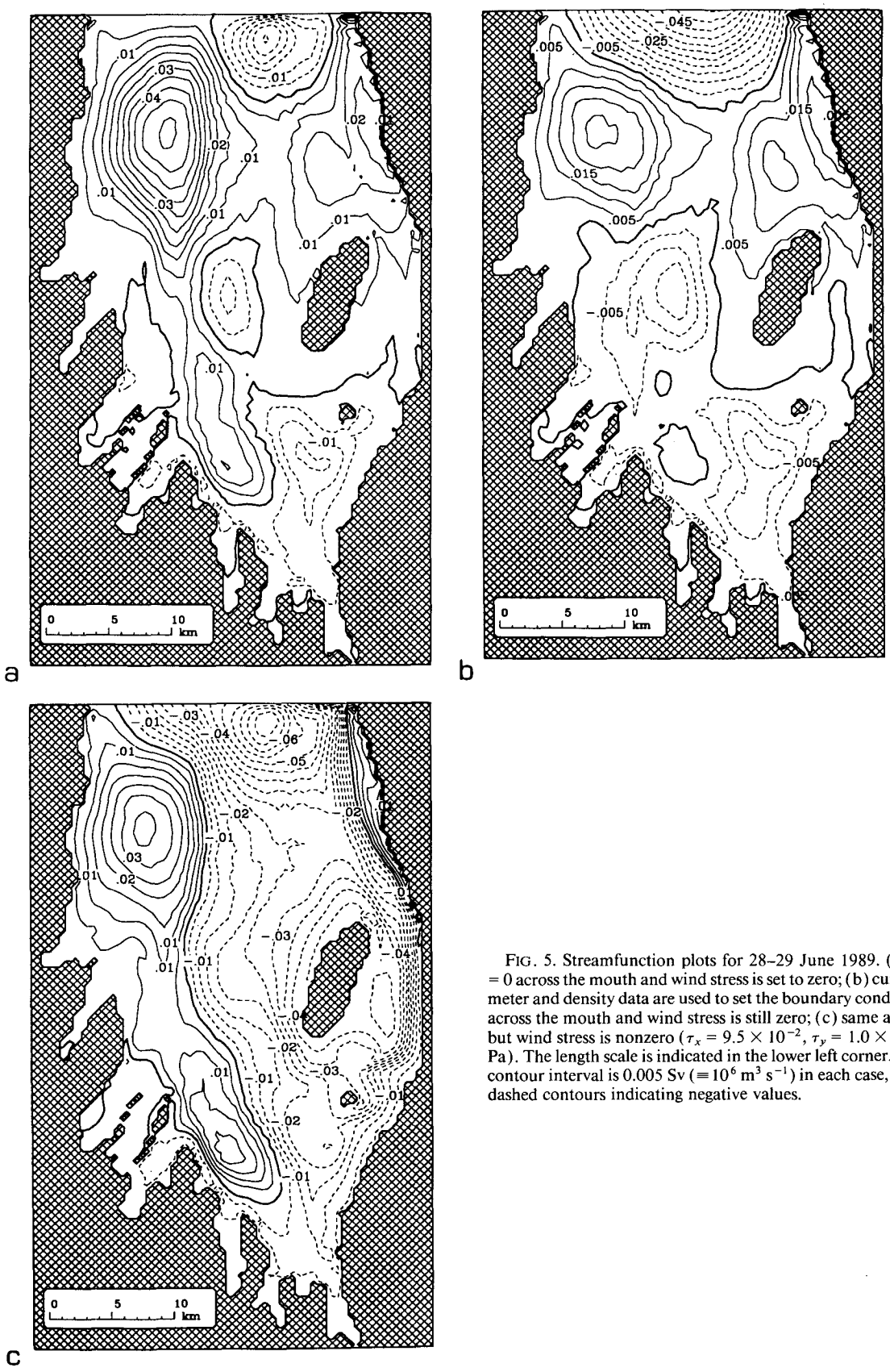

FIG. 5. Streamfunction plots for 28–29 June 1989. (a) $\psi = 0$ across the mouth and wind stress is set to zero; (b) current meter and density data are used to set the boundary condition across the mouth and wind stress is still zero; (c) same as (b) but wind stress is nonzero ($\tau_x = 9.5 \times 10^{-2}$, $\tau_y = 1.0 \times 10^{-1}$ Pa). The length scale is indicated in the lower left corner. The contour interval is 0.005 Sv ($\equiv 10^6$ m^3 s^{-1}) in each case, with dashed contours indicating negative values.

where JEBAR is given by

$$\text{JEBAR} = J\left(\Phi, \frac{1}{H}\right); \tag{16}$$

$J(A, B)$ is the Jacobian operator defined by

$$J(A, B) = -\frac{\partial A}{\partial y}\frac{\partial B}{\partial x} + \frac{\partial A}{\partial x}\frac{\partial B}{\partial y},$$

and Φ is proportional to the potential energy per unit area of the water column and is given by

$$\Phi = H^2 \int_{-1}^{o} b\sigma d\sigma. \tag{17}$$

We now follow Mellor et al. (1982) and Kantha et al. (1982) and introduce a new variable χ defined by

$$\chi = \psi - \Phi/f. \tag{18}$$

Since we are working on an f plane, it follows immediately that (15) can be written as

$$J\left(\chi, \frac{f}{H}\right) = \frac{1}{\rho_o}\left[\frac{\partial}{\partial x}\left(\frac{\tau_s^y - \tau_b^y}{H}\right) - \frac{\partial}{\partial y}\left(\frac{\tau_s^x - \tau_b^x}{H}\right)\right]. \tag{19}$$

The JEBAR term has now been completely absorbed into the left-hand side of the equation. By working with the variable χ, rather than ψ, we avoid having to calculate JEBAR explicitly and hence the problems with noise usually associated with this term (see Mellor et al. 1982).

We must now express the bottom friction (τ_b^x, τ_b^y) in terms of χ, b, and the surface wind stress (τ_s^x, τ_s^y). Since the latter two variables are known inputs to the model, we can then solve (19) for χ. The potential energy can be calculated from the input density field, so once we know χ we also know ψ from (18) and hence the barotropic flow components $\bar{u}$ and $\bar{v}$ from (14). We begin by differentiating (18) to obtain, using (14),

$$\left.\begin{aligned} \frac{\chi_y}{H} &= \bar{u} + \frac{1}{Hf}\Phi_y \\ \frac{\chi_x}{H} &= \bar{v} - \frac{1}{Hf}\Phi_x \end{aligned}\right\}. \tag{20}$$

Writing Φ in terms of z coordinates as

$$\Phi = \int_{-H}^{o} zbdz,$$

the thermal wind relation and integration by parts can be used to show that

$$\left.\begin{aligned} \frac{1}{Hf}\Phi_y &= -\frac{H_y}{f}b_H + u_{gb} - \overline{u_g} \\ \frac{1}{Hf}\Phi_x &= -\frac{H_x}{f}b_H - v_{gb} + \overline{v_g} \end{aligned}\right\}, \tag{21}$$

where b_H is the value of b at the seafloor, $z = -H$. Here (u_g, v_g) is the geostrophic velocity defined by

$$\left.\begin{aligned} -fv_g &= -\frac{1}{\rho_o}\frac{\partial p}{\partial x} - b\sigma\frac{\partial H}{\partial x} \\ fu_g &= -\frac{1}{\rho_o}\frac{\partial p}{\partial y} - b\sigma\frac{\partial H}{\partial y} \end{aligned}\right\}, \tag{22}$$

and overbar denotes vertical average. Substituting into (20) and eliminating $(\bar{u} - \bar{u}_g, \bar{v} - \bar{v}_g)$ using (11), (12), (22), and (10) we now get

$$\begin{aligned} -\frac{\chi_y}{H} &= \frac{\tau_s^y}{\rho_o fH} - \frac{rv_{gb}}{fH} - \frac{H_y b_H}{f} + u_{gb} \\ \frac{\chi_x}{H} &= -\frac{\tau_s^x}{\rho_o fH} + \frac{ru_{gb}}{fH} + \frac{H_x b_H}{f} + v_{gb}, \end{aligned}$$

from which we obtain the following expressions for u_{gb} and v_{gb} in terms of χ, (τ_s^x, τ_s^y) and b

$$\begin{aligned} u_{gb} = \frac{1}{(1+\epsilon^2)}\Bigg[&\left(-\frac{\chi_y}{H} - \frac{\tau_s^y}{\rho_o fH} + \frac{H_y b_H}{f}\right) \\ &+ \epsilon\left(\frac{\chi_x}{H} + \frac{\tau_s^x}{\rho_o fH} - \frac{H_x b_H}{f}\right)\Bigg] \\ v_{gb} = \frac{1}{(1+\epsilon^2)}\Bigg[&\left(\frac{\chi_x}{H} + \frac{\tau_s^x}{\rho_o fH} - \frac{H_x b_H}{f}\right) \\ &- \epsilon\left(-\frac{\chi_y}{H} - \frac{\tau_s^y}{\rho_o fH} + \frac{H_y b_H}{f}\right)\Bigg], \end{aligned} \tag{23}$$

where $\epsilon = r/fH$. Finally, substituting from (23) for (τ_b^x, τ_b^y) in (19) using (10) gives

$$\begin{aligned} &\frac{\partial}{\partial x}\left(\frac{r\chi_x}{(1+\epsilon^2)H^2}\right) + \frac{\partial}{\partial y}\left(\frac{r\chi_y}{(1+\epsilon^2)H^2}\right) \\ &\quad + J\left(\chi, \left\{\frac{f}{H} - \frac{\epsilon r}{(1+\epsilon^2)H^2}\right\}\right) \\ &\qquad = \frac{1}{\rho_o}\left[\frac{\partial}{\partial x}\left(\frac{\tau_s^y}{H}\right) - \frac{\partial}{\partial y}\left(\frac{\tau_s^x}{H}\right)\right] + F, \end{aligned} \tag{24}$$

where

$$\begin{aligned} F = &\frac{\partial}{\partial x}\left(\frac{rH_x b_H}{(1+\epsilon^2)fH}\right) + \frac{\partial}{\partial y}\left(\frac{rH_y b_H}{(1+\epsilon^2)fH}\right) \\ &- J\left(H, \frac{\epsilon r b_H}{f(1+\epsilon^2)H}\right) \\ &- \left[\frac{\partial}{\partial x}\left(\frac{r\tau_s^x}{(1+\epsilon^2)\rho_o fH^2}\right) + \frac{\partial}{\partial y}\left(\frac{r\tau_s^y}{(1+\epsilon^2)\rho_o fH^2}\right)\right] \\ &- \left[\frac{\partial}{\partial x}\left(\frac{\epsilon r\tau_s^y}{\rho_o fH^2(1+\epsilon^2)}\right) - \frac{\partial}{\partial y}\left(\frac{\epsilon r\tau_s^x}{\rho_o fH^2(1+\epsilon^2)}\right)\right]. \end{aligned}$$

This is the equation we solve for χ. The boundary conditions used in the application to Conception Bay

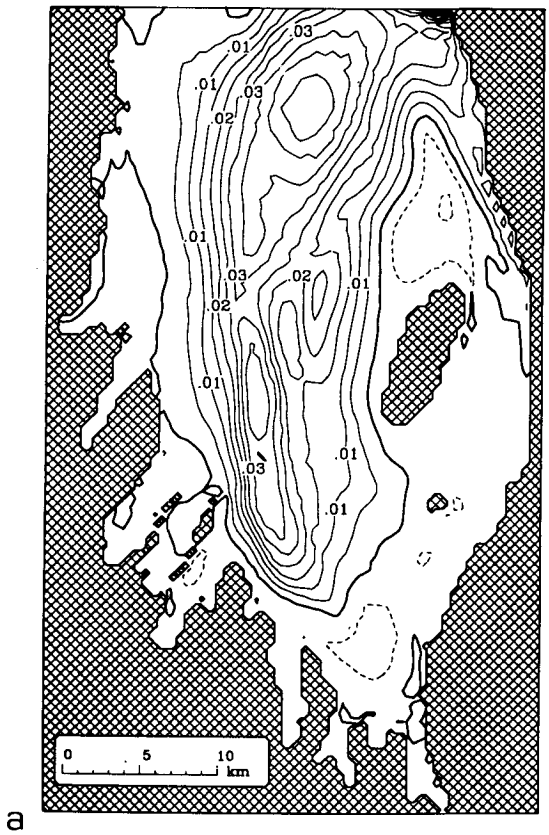

FIG. 6. (a) Streamfunctions for 25 April 1989. The boundary condition across the mouth incorporates wind, density, and current meter data. Wind stress is an average for 24–26 April ($\tau_x = 3.9 \times 10^{-2}$ Pa, $\tau_y = 5.4 \times 10^{-3}$ Pa). The contour interval is 0.005 Sv with dashed contours indicating negative values. (b) Velocity at 2 m. (c) Velocity at 50 m. (d) Velocity at 150 m. (e) Velocity at the bottom, that is, at the lowest σ level. The velocity scale for each plot, in cm s^{-1}, is shown just above the upper-left corner. The thin lines in (c) and (d) are, respectively, the 50- and 150-m isobaths.

are described in the next section where we also discuss the method of solution. In general, the only important restriction in specifying boundary conditions is that χ (and hence ψ, since Φ is known from the density field) must be specified on boundaries where f/H contours enter the model domain (see Greatbatch and Goulding 1992). As already pointed out, once χ is obtained, ψ can be calculated from (18) and then $(\bar{u}, \bar{v})$ from (14).

To calculate the full, three-dimensional velocity field, it remains to solve for that part of (u, v) that has zero vertical average. To do this, we first subtract (11) from (1) and (12) from (2) to obtain

$$-f\hat{v} = -f\hat{v}_g + \frac{1}{H^2}(\nu\hat{u}_\sigma)_\sigma - \frac{(\tau_s^x - \tau_b^x)}{\rho_o H}$$
$$f\hat{u} = f\hat{u}_g + \frac{1}{H^2}(\nu\hat{v}_\sigma)_\sigma - \frac{(\tau_s^y - \tau_b^y)}{\rho_o H}, \tag{25}$$

where carets denote that the vertical average has been removed. Since $(\hat{u}_g, \hat{v}_g)$ can be calculated from b using (3) and (22), and the bottom geostrophic velocity (and hence bottom stress) can be obtained from (23), this equation can be solved for $(\hat{u}, \hat{v})$. Equation (4) is then used to obtain Ω and (5) to obtain the vertical velocity, w, if required.

As we shall show, the preceding method works well in Conception Bay. We have attempted a similar calculation for the North Atlantic using the Levitus (1982) density data. In this case the method failed because to obtain ψ from χ using (18) involves subtracting two terms (χ and Φ/f) that in the North Atlantic are both many orders of magnitude larger than ψ. It follows that any error in the calculation of χ [in particular from the terms labeled F in (24)] will swamp the streamfunction, ψ, as indeed seems to be the case. We conclude that the method works as long as χ, ψ, and Φ/f all have the same magnitude. In a bay like Conception Bay, this is the case, but over the whole North Atlantic it is not. [It is possible that the North Atlantic calculation would work if sufficient resolution was used to ensure that the term labeled F in (24) could be calculated accurately.]

One final point to note: Putting $\epsilon = 0$ in (24), and using (18) to express χ in terms of ψ and Φ, gives the steady-state version of Eq. (22) for ψ in Mertz and Wright (1992). Similar equations for ψ when bottom friction is expressed in terms of either bottom geostrophic velocity or bottom velocity are given by Eqs. (26) and (50) in Greatbatch and Goulding (1992). Our Eq. (24) has the advantage that the often troublesome JEBAR term does not appear explicitly and, therefore, does not have to be calculated. Mertz and Wright (1992) point out that the JEBAR term also does not appear explicitly in the equation for the vertical component of the curl of the vertically integrated

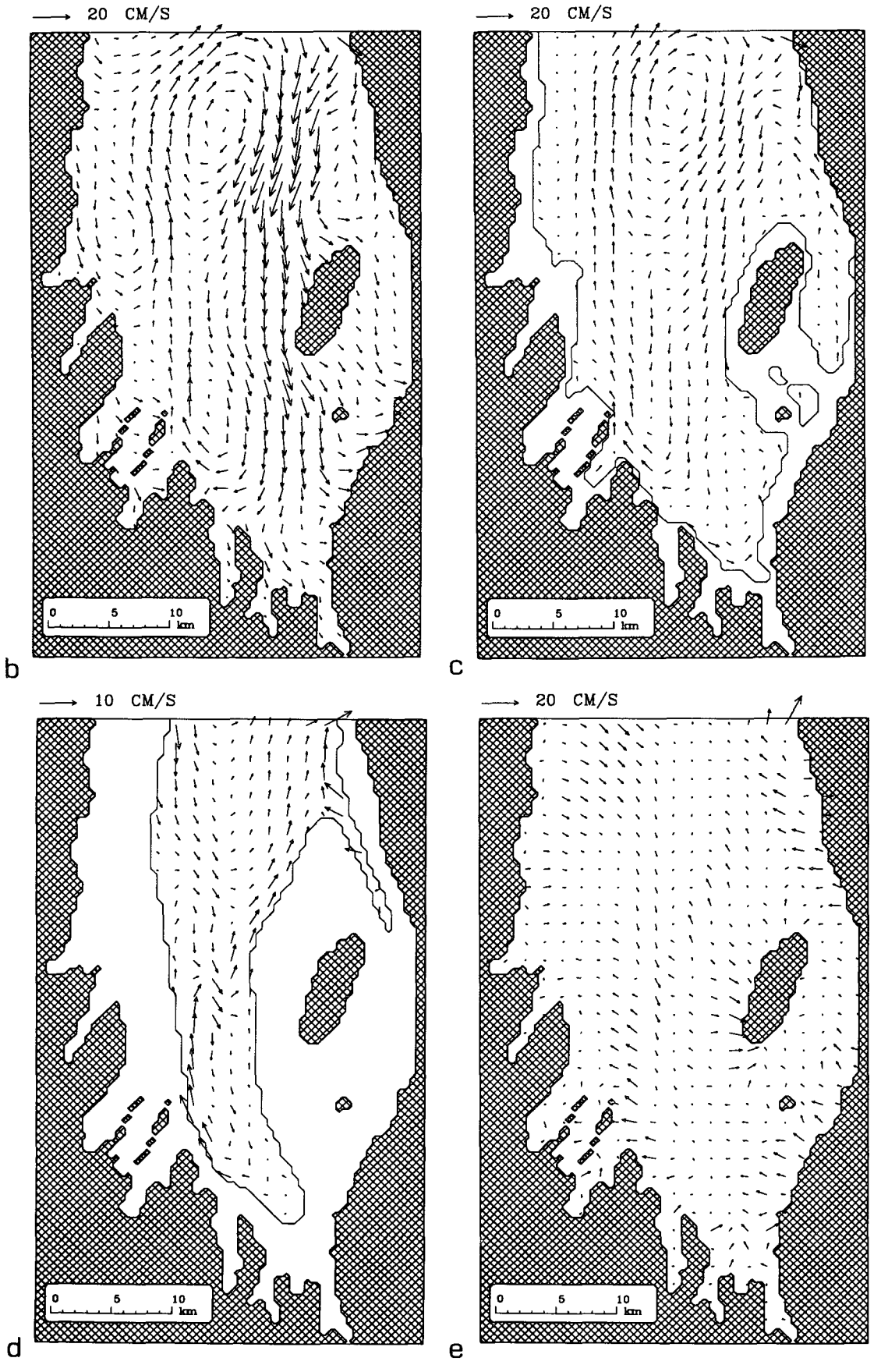

FIG. 6. (*Continued*)

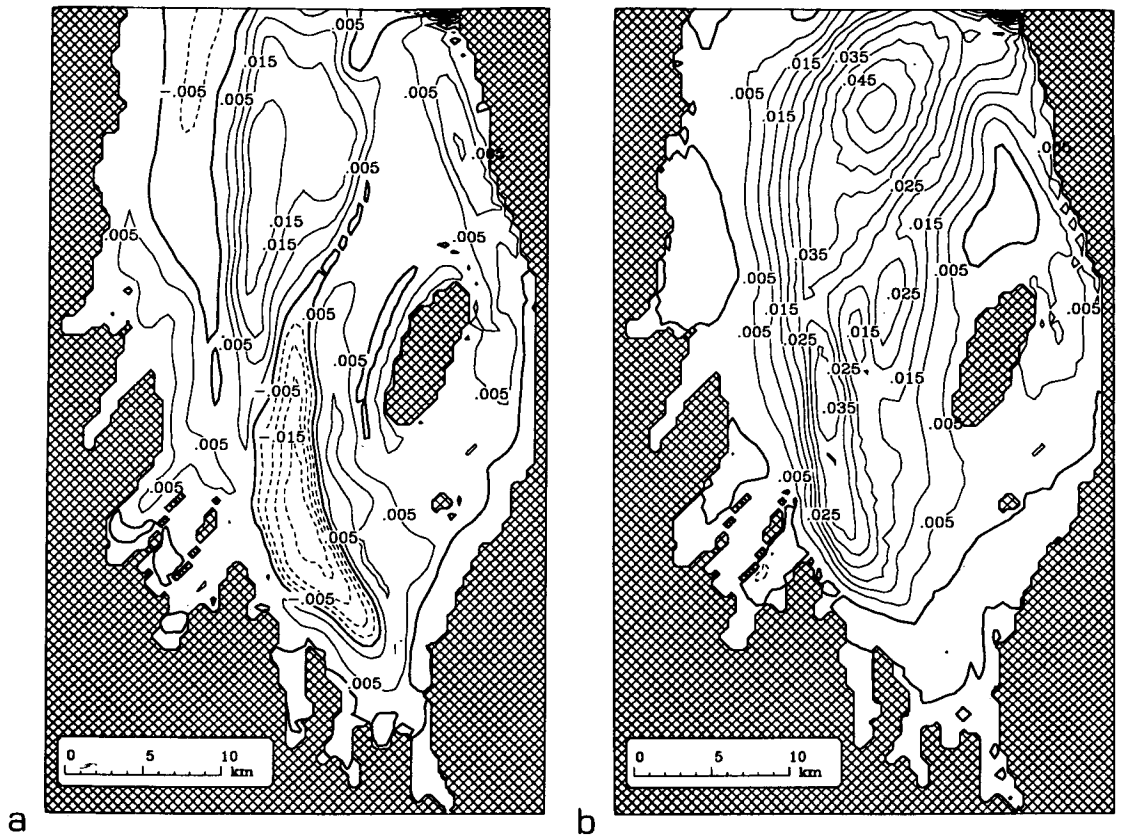

FIG. 7. For the 25 April 1989 case, (a) χ and (b) streamfunction. No wind stress is applied to these results. The contour interval is 0.005 Sv with negative contours indicating negative values.

(as distinct from vertically averaged) momentum equations. Instead, a term involving the bottom pressure torque is obtained, as discussed by Holland (1973) and Greatbatch et al. (1991). This approach to dealing with JEBAR, which involves solving for the bottom pressure, is essentially that taken by Rattray (1982).

3. The method of solution

The model domain and bottom topography used in the application to Conception Bay are shown in Fig. 1. To solve for χ, (24) is written in finite-difference form and the resulting matrix equation is solved using the method of Lindzen and Kuo (1969). Land areas are treated as shallow water of depth 1.0 m with each of the terms involving the wind stress being set to zero over the land and b_H taking values extrapolated (in the z-coordinate domain) from the surface density values in the bay. The boundary conditions on χ are applied around the edge of the solution domain (a rectangle in x, y space). Apart from the boundary that runs across the mouth of the bay, the model boundaries all occur over the land; χ is set to zero along these boundaries. Since Φ is zero over land, this is equivalent to setting $\psi = 0$ along these boundaries, as can be seen from (18). Across the mouth of the bay, ψ is specified, that is, $\psi = \psi_N$, with ψ_N given as an input to the model. The corresponding boundary condition on χ is $\chi = \psi_N - \Phi_N/f$, where Φ_N is Φ along the northern boundary. A five-point Laplacian is used to finite difference the Laplacian term in (24).

The finite differencing of the remaining equations [i.e., (25) and (4)] is the same as in Greatbatch and Goulding (1992). The grid arrangement is shown in Fig. 2. In the horizontal, this is the Arakawa B grid (see Mesinger and Arakawa 1976). To finite difference the horizontal pressure gradient terms we use the method of Blumberg and Mellor (1987). We therefore define two new functions $A(x, y, \sigma)$ and $B(x, y, \sigma)$ by

$$\left.\begin{aligned} A &= \int_\sigma^o b\,d\sigma \\ B &= \int_\sigma^o \sigma \frac{\partial b}{\partial \sigma}\,d\sigma \end{aligned}\right\}. \tag{26}$$

Using integration by parts, it is easy to see that

$$B = -\sigma b - A. \tag{27}$$

Also, integrating (3) we see that

$$p = p_s + \rho_o HA, \tag{28}$$

where p_s is the surface pressure (at $\sigma = 0$). Using (27) and (28), we now see that

$$\left.\begin{aligned} \left.\frac{\partial p}{\partial x}\right|_z &= \left.\frac{\partial p}{\partial x}\right|_\sigma + \rho_o b\sigma \frac{\partial H}{\partial x} = \frac{\partial p_s}{\partial x} + \rho_o\{HA_x - H_x B\} \\ \left.\frac{\partial p}{\partial y}\right|_z &= \left.\frac{\partial p}{\partial y}\right|_\sigma + \rho_o b\sigma \frac{\partial H}{\partial y} = \frac{\partial p_s}{\partial y} + \rho_o\{HA_y - H_y B\} \end{aligned}\right\}. \tag{29}$$

The horizontal pressure gradient terms are now obtained by finite differencing the expressions involving A and B on the right-hand side of (29). This has the advantage that if b is a linear function of z, and does not depend on x and y, then the finite-difference expressions for $(HA_x - H_x B)$ and $(HA_y - H_y B)$ are exactly zero, no matter how steep the bottom topography, and in agreement with their analytic equivalents for this b. This addresses the problem raised by Haney (1991), but unfortunately only eliminates the error completely in this special case.

The calculations to be described using data from Conception Bay use a grid resolution of 0.5 km in x and y and 40 equally spaced σ levels in the vertical.

4. The Conception Bay dataset used as input to the model

Conception Bay is a large coastal embayment on the east coast of the island of Newfoundland (Fig. 1). It is approximately 70 km long, 32 km across at the mouth, with a maximum depth in the center of about 300 m. There is a sill about 150 m deep, at the mouth of the bay, which restricts access and closes off isobaths (and hence f/H contours) inside the bay. For the purposes of this study, we shall consider the mouth to be along the line of moorings M3, M4, M5, M6 shown in Fig. 3. The bottom topography of the bay, shown at 0.5-km resolution in Fig. 1, shows the deep basin with an irregular coastline and a number of small islands. An oceanographic study, both biological and physical, was conducted in the bay from 1986 to 1991. A summary and discussion of the physical data can be found in deYoung and Sanderson (1992).

The density data used as input to the model are constructed from CTD sections taken in the bay in 1989, together with one case from 1990. Different datasets were constructed from different surveys in order to use the model to infer circulation changes in the bay. The stations used in the CTD surveys are shown in Fig. 3. Each survey took 1–2 days to complete. This raises the possibility that the data may be aliased. We do not think, however, that this is a serious problem. For example, the tides in Conception Bay are quite weak with constituent velocities less than 0.02 m s^{-1} (deYoung and Sanderson 1992) so that aliasing caused by tidal effects should be small. In addition, spectra of both currents and temperature measured at moorings in the bay (see Fig. 3) are quite "red" with most of the energy at periods of 2–10 days. Furthermore, model-computed surface velocities look quite similar, in terms of their features and scales, to surface velocities obtained using a two-site HF radar system (CODAR: Coastal Ocean Dynamics Applications Radar; Barrick et al. 1977). This gives us confidence that the model-computed velocity fields are meaningful. This whole issue is discussed further in section 5.

We noted in section 3, that the local time derivative and nonlinear terms in the momentum equations are neglected from the model. The preceding discussion provides some justification for neglecting the former. Consistency checks on our solutions suggest that the Rossby number may locally be as high as 0.2 for our diagnosed flows, suggesting some possible role for the nonlinear terms. Clearly, however, their effect is unlikely to be very great and it seems reasonable to proceed with these terms neglected.

To use the density data as input to the model, it is necessary to map it to a grid with the same resolution as the model—in this case 0.5 km in the horizontal and 40 equally spaced sigma levels in the vertical. This was done in two stages, first mapping the data to a 0.5-km grid in z coordinates with 1-m vertical resolution. These data were then transferred onto the grid in sigma coordinates using linear interpolation. It was found in the course of the analysis that there was some sensitivity of the model results to noise in the density field. Surface data were particularly difficult to treat. CTD data were obtained using Seabird SBE25 and/or Neil Brown MK III probes, with σ_t accurate to better than ± 0.01. Data from these probes were averaged, by separately combining temperature and conductivity and then recomputing salinity, to minimize the effects of salinity spiking. The remaining data at vertical resolutions of 5–10 cm were then averaged to yield profiles at 1-m intervals. These 1-m-averaged data regularly had spikes in the near-surface data (0–10 m) that were removed and replaced by linear interpolation. These "cleaned-up" 1-m data were gridded using a Kriging technique in z coordinates and then transformed into σ coordinates. There are 40 σ levels in the model so the vertical resolution varies between 0.5 m and 5 m, being least in the deepest part of the bay.

Figure 4a shows a sample of the density along the axis of the bay for 25 April 1989. The station separation is roughly 7 km. There is an alongaxis density gradient in the surface, with warmer, less saline water at the head of the bay. A broad pycnocline is present that spreads vertically toward the mouth of the bay. A line across the middle of the bay (Fig. 4b) shows that there is also cross-bay structure. It should be noted that the cross-bay resolution is much better than the alongbay—about 4 km here.

Some of the model calculations include surface wind forcing. Wind data are not available for Conception

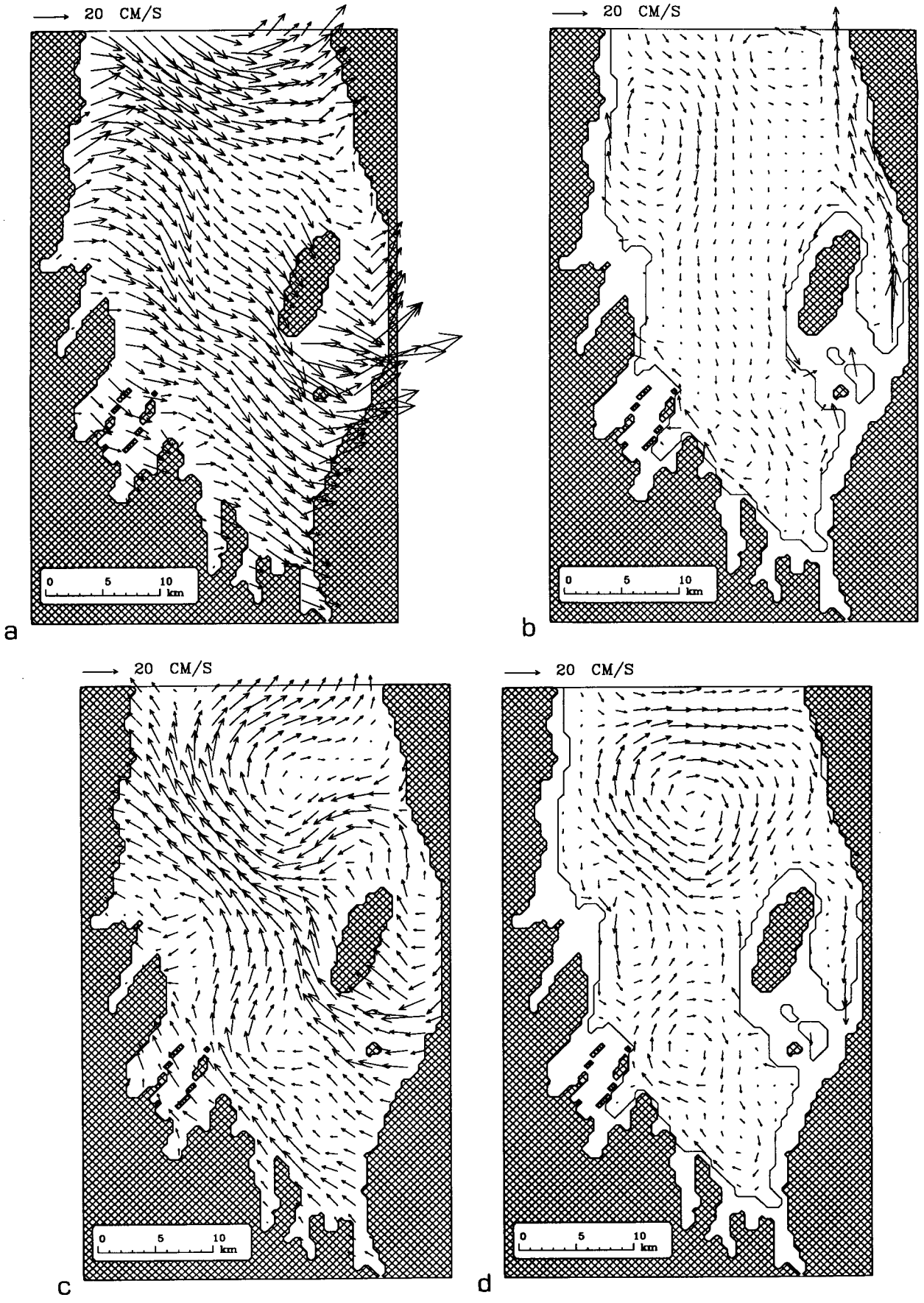
20 CM/S
0 5 10 km
a
20 CM/S
0 5 10 km
b
20 CM/S
0 5 10 km
c
20 CM/S
0 5 10 km
d

Bay itself, so data from the nearest available station, St. John's Airport about 20 km to the southeast, were used instead. Comparisons between the wind at St. John's and a short record from a station at the head of the bay show that the wind at St. John's is well correlated to the Conception Bay wind. DeYoung et al. (1992) and Otterson (1992) have used these data to drive a reduced-gravity model of the bay and have shown that it successfully reproduces upwelling events occurring in the pycnocline of the bay. Wind stress was calculated using the formula of Large and Pond (1981). Averages of wind stress over 2.5-day periods corresponding to the time of the CTD surveys were then obtained and these averages used as input to the model.

We now describe the boundary conditions used in the model along the open boundary across the mouth of the bay. The simplest boundary condition is one of no transport through the boundary, corresponding to putting ψ_N in section 3 equal to zero. However, to take some account of flow into and out of the bay, three other boundary conditions were also used and separately calculated. For the first boundary condition, geostrophic transport relative to the bottom was obtained using density data from along the model boundary. This was then corrected by adding the least-squares nonzero bottom velocities necessary to ensure that there is no net transport into or out of the bay. This adjustment gives bottom velocities as high as 0.1 m s^{-1}. The second boundary condition used data from the line of current meter moorings along the boundary (see Fig. 3) to add a barotropic component to the flow through the boundary. The mean velocity during the time period of each CTD survey was calculated for the deepest current meter on each mooring (depth approximately 100 m). These average velocities were then used as reference velocities for geostrophic calculations of the velocity field at each mooring. Between moorings, linear interpolation was used to obtain both the reference velocities and also the reference depths. Extrapolation from the last mooring to the coast was done by assuming that the bottom velocity at the coast is zero and interpolating as before. In regions where the bottom is shallower than the interpolated depth, the bottom velocity was obtained by assuming a linear relation between bottom depth and bottom velocity. This velocity field was then corrected in a least-squares sense, as before, to ensure no net transport through the boundary. Finally, wind-driven Ekman transport was included and least-squares velocities added as before, to obtain the third boundary condition.

The eddy viscosity used in the calculations is $\nu = 10^{-3}$ m^2 s^{-1}, corresponding to an Ekman layer depth of roughly 5 m. Two other values were used in tests (10^{-2} m^2 s^{-1} and 10^{-4} m^2 s^{-1}) and did not give significantly different results. It should be noted that since bottom stress is given in terms of bottom geostrophic velocity, the calculated volume transport streamfunction is independent of the eddy viscosity. The primary effect of varying ν is to change the depth of the surface and bottom Ekman layers. The flow will remain dominated by the geostrophic flow in the interior provided the vertical geostrophic shear occurs on length scales that are large compared with the Ekman layer depth, as is the case for our solutions. The value of the bottom friction coefficient used is $r = 0.0005$ m s^{-1}. Both this and the value for the vertical eddy viscosity are reasonable for most shelf regions (Csanady 1982).

Finally, the bottom topography used in the model was obtained from bathymetric charts at a resolution of 0.5 km and then smoothed using a Gaussian smoother with length scale 1 km.

5. Model results

Three different model-calculated streamfunctions for 28–29 June 1989 are shown in Fig. 5. Figure 5a is calculated using the boundary condition $\psi = 0$ across the mouth and with the surface wind stress set to zero. A number of eddylike features are apparent in the bay, with length scales of 5–10 km. Figure 5b shows the streamfunction when both the current meter and the density data are used to determine the boundary condition at the mouth. The eddy features can still be identified, but now there is a strong inflow at the western side of the bay and outflow on the eastern side. Although the interior ψ is clearly modified by this inflow, the streamlines that originate at the mouth do not penetrate far into the bay. Adding wind stress further modifies the streamfunction (Fig. 5c), especially in the shallow regions of the bay around Bell Island. Streamlines now penetrate from the mouth all the way to the head of the bay. Note that the wind stress is fixed in the model and is a 2-day average centered about the time of collection of the density data.

We now examine in more detail the results of calculations done using data from the 25 April 1989 survey. Figure 6 shows model-calculated streamfunctions and velocities at several different depths, including the bottom. In this case, the boundary condition at the mouth includes all three influences, that is, the density field, the current meter data, and the surface wind

FIG. 8. Velocity at (a) 2 m and (b) 50 m for 28–29 June 1989. These velocities correspond to the streamfunction presented in Fig. 5c. The boundary condition across the mouth incorporates wind, density, and current meter data. (c) Velocity at 2 m and (d) 50 m for 17 April 1989. The boundary condition across the mouth incorporates wind, density, and current meter data. The velocity scale for each plot is shown just above the upper-left corner.

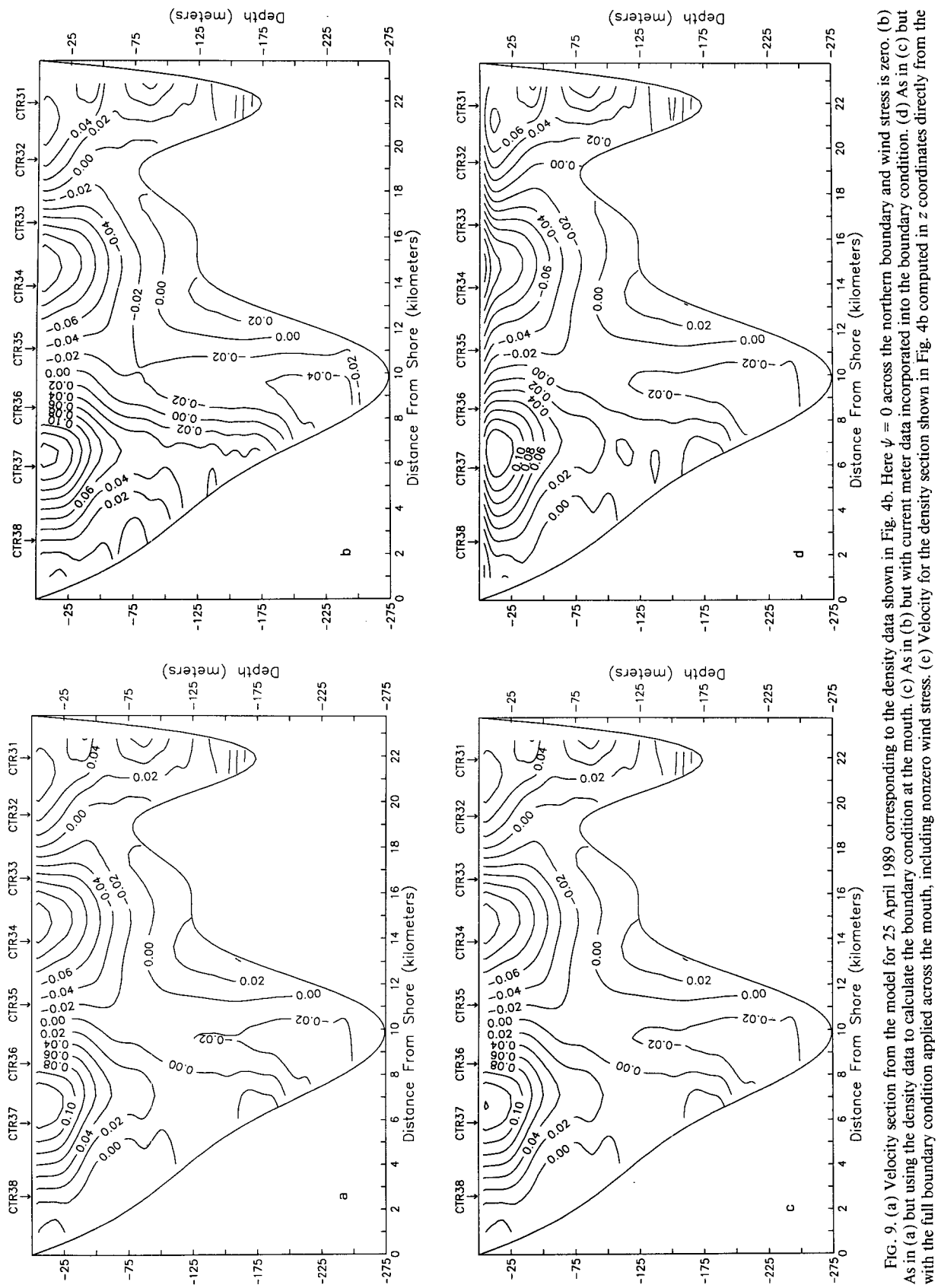

FIG. 9. (a) Velocity section from the model for 25 April 1989 corresponding to the density data shown in Fig. 4b. Here $\psi = 0$ across the northern boundary and wind stress is zero. (b) As in (a) but using the density data to calculate the boundary condition at the mouth. (c) As in (b) but with current meter data incorporated into the boundary condition. (d) As in (c) but with the full boundary condition applied across the mouth, including nonzero wind stress. (e) Velocity for the density section shown in Fig. 4b computed in z coordinates directly from the

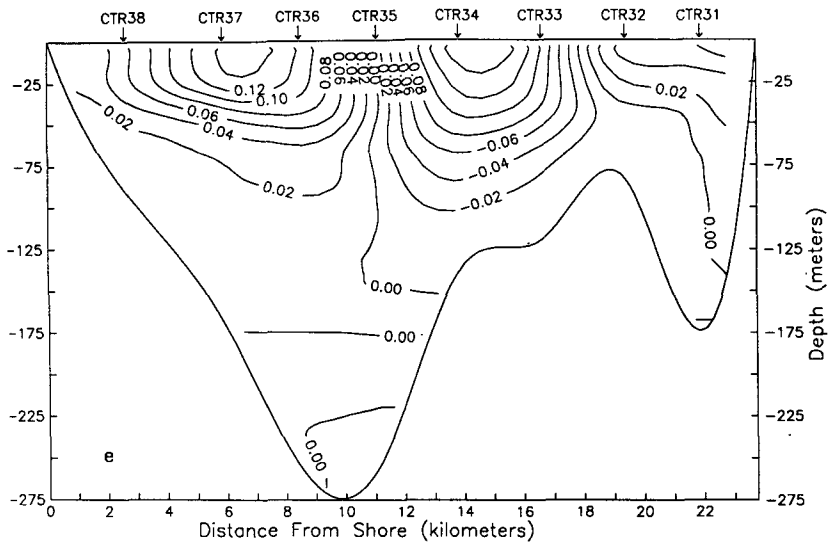

FIG. 9 (*Continued*) data using the dynamic method of Helland-Hansen (1934). Velocities here are in m s^{-1}.

stress. For this survey, the winds were rather weak with the mean wind stress used in the model being from the southwest with a magnitude of 3.9×10^{-2} Pa. As in the 28 June case, the wind plays an important role in shallow water, but is less influential in the deeper parts of the bay. For example, comparing the velocities at a depth of 2 m (Fig. 6b) with those at 50 m (Fig. 6c), we see that although there is a reduction in the magnitude of the velocity, the direction is similar at both depths over much of the bay. Comparing with the velocities at a depth of 150 m (Fig. 6d), we see that the large eddy just in from the open boundary has strong baroclinic structure, whereas that near the head of the bay is much more barotropic.

To gain some insight into the dynamics, Fig. 7a shows a plot of χ as defined by (18) and calculated for the same case as in Fig. 6 but with the wind stress set equal to zero. Looking for regions where χ contours in Fig. 7a cross the depth contours in Fig. 1 tells us where the torque due to (τ_b/H) is important. This follows from Eq. (19) since the wind stress is zero. It is clear that χ changes considerably as one moves from the mouth to the head of the bay, indicating an important role for this torque. On the other hand, the streamfunction, shown in Fig. 7b, much more closely follows the depth contours (apart from near the mouth), suggesting that in this particular example, the torque due to τ_b/H is largely balanced by the JEBAR term [see Eq. (15) with the wind stress set to zero]. An important role for the bottom stress torque $(\partial\tau_b^y/\partial x - \partial\tau_b^x/\partial y)$ is indicated by the large regions of convergence and divergence apparent in the bottom velocity from Fig. 6e. Since the horizontal divergence of the overlying geostrophic flow must be zero, these regions of convergence and divergence must be balanced by horizontal geostrophic flow toward or away from the sloping topography—an interesting example of how in a rotating fluid, the Ekman layers can exert a strong influence on the flow even though they occupy only a small fraction of the water column.

Model-calculated surface and subsurface currents for two different periods are shown in Fig. 8. Relatively strong southwesterly winds were present in the 28–29 June case (Fig. 8a,b), the wind-stress magnitude $|\tau| = 0.14$ Pa corresponding to a wind speed of roughly 10 m s^{-1}. This drives a strong surface Ekman flow across the bay (Fig. 8a). Below the surface, at 50 m, there is a much different circulation with inflow along the northwest side of the bay and outflow along the southeast side. Surface velocity from 17 April 1989 (Fig. 8c) is quite different. In this case, there is a strong northeasterly wind of $|\tau| = 8.1 \times 10^{-2}$ Pa blowing inwards along the axis of the bay. As a consequence, cross-bay surface flow is toward the northwest, and a gyre, which is visible near the mouth at 50 m (Fig. 8d), is substantially modified at 2 m. Also, we do not see the strong outflow on the southeast side of the bay we saw in Fig. 8a.

One other way to investigate the model results and to test sensitivity is to compare model output along a section using different inflow boundary conditions. We can also compare our results with calculations made using the dynamic method, that is, with the geostrophic velocity referenced to the bottom. By carrying out the dynamic velocity calculation in z coordinates, this also provides a check on the accuracy with which the horizontal pressure gradients are being calculated by the model in the σ coordinate system (Haney 1991). Figure 9 shows velocity extracted from the 25 April model run (of Fig. 6) along the C31 to C37 line (the density data from this section are shown in Fig. 4b). The model results were interpolated onto the C3 line and the ve-

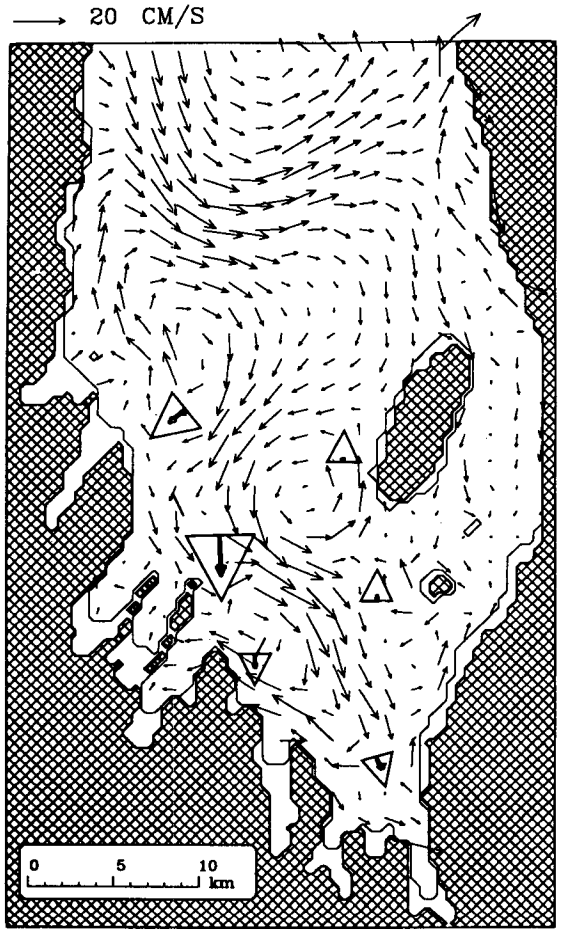

FIG. 10. Model-calculated velocity at a depth of 20 m based on survey data from 22 June 1990. Also shown are velocities measured by current meters averaged over the same time period and at roughly the same depth. These are shown by bold arrows enclosed by triangles that point in the direction of the flow.

locity component perpendicular to the line was extracted. Here positive velocity is out of the bay and negative velocity is into the bay. Figure 9a shows the velocity for the simplest version of the model, where $\psi = 0$ across the northern boundary. We see inflow centered near station 34 and outflow near station 37. Changing the boundary condition at the mouth to include information from the density field along the boundary leads to changes at depth in the western part of the section (Fig. 9b). There is now stronger, more barotropic outflow near station 37 that is compensated by deep inflow near the base of the western slope at the deepest part of the section. Adding information from the current meters at the mouth (Fig. 9c) weakens these flows and leads to a picture very like that in Fig. 9a. Adding surface wind stress (Fig. 9d) modifies this only slightly, except near the surface where the wind-driven Ekman transport is now important. Figure 9e shows the dynamic velocity, calculated in z coordinates, after extrapolating isopycnals horizontally under the bottom from their point of intersection with the topographic slope (the method of Helland-Hansen 1934). The overall structure is very similar to that in the other figures, the differences being due to the fact that the velocity at the bottom is zero, whereas in the model it is, in general, nonzero. This gives us confidence in our results and, in particular, indicates that the error in computing the horizontal pressure gradient terms in the σ coordinate system is within acceptable limits.

One of the things that can be done with the model results is to compare them with observed current meter data. Figure 10 shows a comparison between the model-computed velocity field at a depth of 20 m and data from current meters nominally at that depth and averaged over the two-day survey period (note that the current meter data had first been low-pass filtered to remove energy at periods below 1.5 days). It is clear that while the agreement is not spectacular, there is certainly some similarity between the computed and measured velocities. For example, at moorings H1 and H2 (see Fig. 3), we can see the influence of the eddies to the west of Bell Island. Agreement is least satisfactory at those moorings close to the shore (e.g., mooring H3). This suggests the influence of baroclinic Kelvin waves propagating in the coastal waveguide (the radius of deformation is near 5 km, so the influence of these waves should be confined near the coast). Evidence for the presence of these waves is given by Otterson (1992) and de Young et al. (1992).

Finally, in Fig. 11, we show surface velocities obtained using CODAR (see Barrick et al. 1977). The two radar sites used to obtain these results are shown by the star on the west coast of the bay. Unfortunately we do not have any CODAR data from time periods coincident with the CTD surveys. This means that we cannot directly compare CODAR-derived and model-calculated velocities. It is clear from Fig. 11, however, that the structure and scales of the features obtained from the model calculations agree well with those identified by CODAR.

6. Summary and discussion

A diagnostic numerical model to compute the 3D velocity field from a specified density field has been described. The model allows velocity to be computed without the ambiguous extrapolations necessary in the "classical" technique of dynamic height calculations. The model is an extension of that of Mellor et al. (1982) to include vertical mixing and bottom friction and to allow calculation of the velocity field inside regions of closed f/H contours. It takes advantage of the change of dependent variable introduced by Mellor et al. (1982) to avoid explicit calculation of the JEBAR term (the joint effect of baroclinicity and relief; Sarkisyan and Ivanov 1971).

There are a number of nice features associated with using the model.

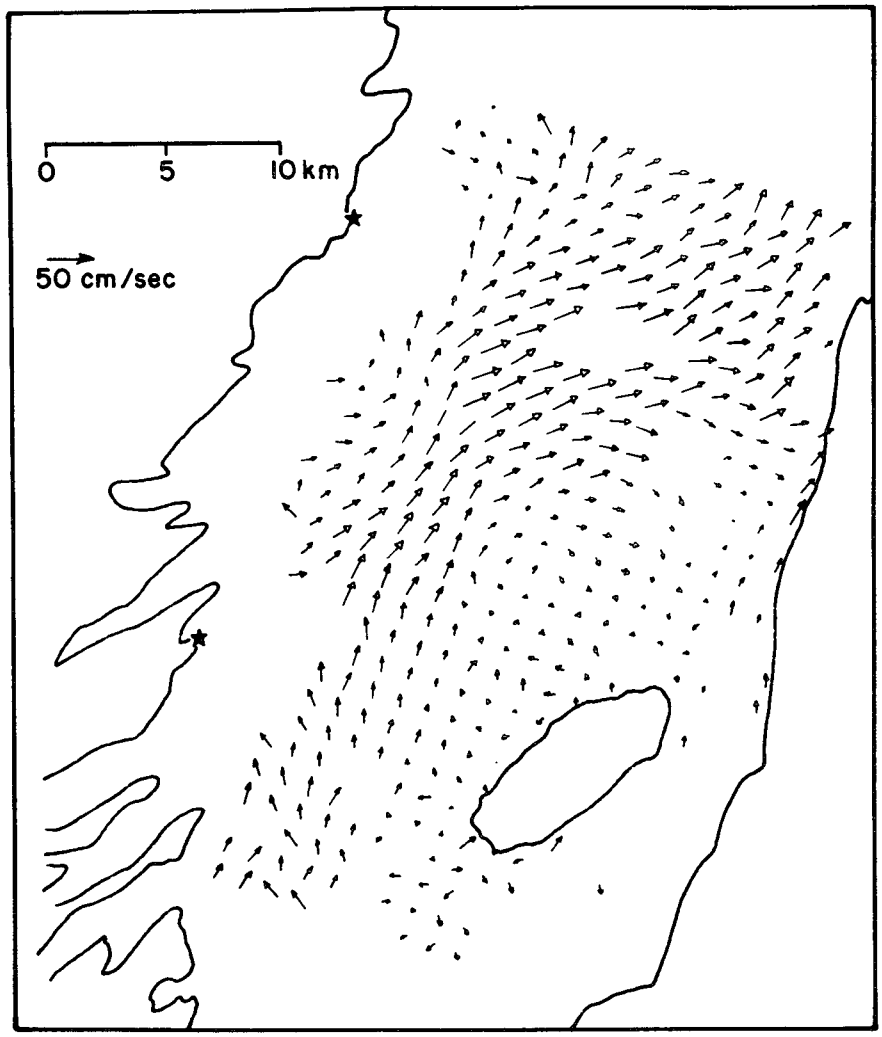

FIG. 11. Surface velocity derived from CODAR at 0000 UTC 7 July 1989. The two radar sites are shown by a star.

1) It is computationally efficient and easy to implement.

2) The computed velocity field is consistent; in particular, it satisfies the steady, linearized momentum equations and the continuity equation.

3) There is no need to extrapolate the density field below the bottom as in the dynamic height method.

4) The JEBAR term does not need to be calculated explicitly.

5) Bottom stress is included, although it must be parameterized in terms of bottom geostrophic velocity.

6) Wind stress can be included.

7) Vertical eddy viscosity is included.

8) Boundary conditions based on observed data can be easily incorporated.

9) The model can be used in regions with closed f/H contours, where f is the Coriolis parameter and H is the ocean depth.

The chief weaknesses of the model are that the density field must be specified and that the local time derivative and nonlinear terms must be neglected from the momentum equations. To deal with the former, a technique such as objective analysis (e.g., Levitus 1982) is required to produce a density field that can be transferred to the model grid. A much better method would be to use a prognostic model and to assimilate the data into the model using a 4D data assimilation technique. This would produce both a density and velocity field that would be consistent with the model equations and would "fit" the measured data in some sense (e.g., a least-squares fit). This avoids the use of a technique such as objective analysis, which takes no account of dynamics and would also allow us to include the local time derivative and nonlinear terms in the momentum equations. On the other hand, such an approach is very ambitious (e.g., see Tziperman et al. 1992a,b) and is

beyond the scope of the present paper. By contrast, it is the principal advantage of our model that it is computationally very efficient and easy to implement and, as such, is a cheap and convenient way to obtain information on the circulation.

The model as described in this paper uses a normalized depth (i.e., σ) coordinate in the vertical, in common with the 3D prognostic model of Blumberg and Mellor (1987). However, it is important to note that the method would work just as well if the vertical structure was calculated using a z coordinate formulation (this would have the advantage of eliminating the error that can arise when calculating the horizontal pressure gradient terms in the σ coordinate system; Haney 1991). Indeed, the equation we solve to determine the vertically averaged component of the flow, that is, Eq. (24), is independent of the choice of vertical coordinate.

We illustrated the use of the model by applying it to data collected in Conception Bay, Newfoundland. The model-computed surface velocity exhibits the same scales and features as surface velocity derived from CODAR data (Barrick et al. 1977).

The model is easily adaptable to different areas, needing only bottom topography, density, and wind data. For the example of Conception Bay, we also used data from current meters to constrain the boundary condition at the mouth. However, it is best suited to shelf regions where horizontal variations in the density field and the Coriolis parameter are not large. We are in the process of applying an updated version of the model to the Newfoundland shelf and slope, where strong geostrophic flows should permit detailed comparisons with current meter data.

Acknowledgments. This work has been funded by the Natural Sciences and Engineering Research Council of Canada (NSERC) through a Strategic Grant (the Cold Ocean Productivity Experiment) and through OPEN, one of the 15 Networks of Centres of Excellence supported by the Government of Canada. Early work on this project was also supported by a Department of Supply and Services Contract awarded to R. Greatbatch through Moto Ikeda at the Bedford Institute of Oceanography. We are grateful to Moto Ikeda for his support and also to Allan Goulding, Ken Munro, and Ying Ren for their assistance. Joy Simmons typed the original version of the manuscript and we are grateful to Jim Helbig of the Department of Fisheries and Oceans for access to the CODAR data.

REFERENCES

Barrick, D. E., M. W. Evans, and B. L. Weber, 1977: Ocean surface currents mapped by radar. *Science,* **198,** 138–144.

Blumberg, A., and G. L. Mellor, 1987: A description of a three-dimensional coastal ocean circulation model. *Three Dimensional Coastal Ocean Models, Coastal and Estuarine Science Series,* Vol. 4, N. Heaps, Ed., Amer. Geophys. Union, 1–16.

Bryan, K., 1969: A numerical method for the study of the circulation of the world ocean. *J. Comput. Phys.,* **4,** 347–376.

Csanady, G. T., 1979: The pressure field along the western margin of the North Atlantic. *J. Geophys. Res.,* **84,** 4905–4915.

——, 1982: *Circulation in the Coastal Ocean.* Reidel, 279 pp.

deYoung, B., and B. Sanderson, 1992: Seasonal cycles and mean circulation in Conception Bay, Newfoundland. *Atmos.–Ocean,* submitted.

——, T. Otterson, and R. J. Greatbatch, 1993: The local and nonlocal response of Conception Bay to wind forcing. *J. Phys. Oceanogr.,* **23,** 2636–2649.

Greatbatch, R. J., and A. Goulding, 1992: A long-time scale, density-stratified shelf circulation model. *Contin. Shelf Res.,* **12**(1), 115–141.

——, A. F. Fanning, A. G. Goulding, and S. Levitus, 1991: A diagnosis of interpentadal circulation changes in the North Atlantic. *J. Geophys. Res.,* **96**(C12), 22 009–22 023.

Groen, P., 1948: Methods for estimating dynamic slopes and currents in shallow water. *J. Mar. Res.,* **7,** 313–316.

Haney, R. L., 1991: On the pressure gradient force over steep topography in sigma coordinate models. *J. Phys. Oceanogr.,* **21,** 610–619.

Helland-Hansen, B., 1934: The Sognefjord section-Oceanographic observations in the northernmost part of the North Sea and the southern part of the Norwegian Sea. *James Johnstone Memorial Volume,* Lancashire Sea-Fish Lab. [Available from the Proudman Oceanographic Laboratory, Bidston Observatory, Birkenhead, U.K.]

Herring, H. J., and L. H. Kantha, 1990: *Climatological Atlas for the Eastern Continental Shelf.* Dynalysis of Princeton, 94 pp.

Holland, W. R., 1973: Baroclinic and topographic influences on the transport of western boundary currents. *Geophys. Fluid Dyn.,* **4,** 187–210.

——, and A. D. Hirschman, 1972: A numerical calculation of the circulation in the North Atlantic Ocean. *J. Phys. Oceanogr.,* **2,** 336–354.

Kantha, L. H., G. L. Mellor, and A. F. Blumberg, 1982: A diagnostic calculation of the general circulation in the South Atlantic Bight. *J. Phys. Oceanogr.,* **12,** 805–819.

Large, W., and S. Pond, 1981: Open ocean momentum flux measurements in moderate to strong winds. *J. Phys. Oceanogr.,* **11,** 324–336.

Lazier, J. R. N., and D. G. Wright, 1993: Annual velocity variations in the Labrador Current. *J. Phys. Oceanogr.,* **23,** 659–678.

Levitus, S., 1982: *Climatological Atlas of the World Ocean.* NOAA Prof. Pap., 13, Natl. Oceanic and Atmos. Admin., Washington, D.C., 173 pp.

Lindzen, R. S., and H. L. Kuo, 1969: A reliable method for the integration of a large-class of ordinary and partial differential equations. *Mon. Wea. Rev.,* **97,** 732–734.

Lynch, D. R., F. E. Werner, D. A. Greenberg, and J. W. Loder, 1992: Diagnostic model for baroclinic, wind-driven and tidal circulation in shallow seas. *Contin. Shelf Res.,* **12**(1), 37–64.

Mellor, G. L., C. R. Mechoso, and E. Keto, 1982: A diagnostic calculation of the general circulation of the Atlantic Ocean. *Deep-Sea Res.,* **20,** 1171–1192.

Mertz, G., and D. G. Wright, 1992: Interpretations of the JEBAR term. *J. Phys. Oceanogr.,* **22,** 301–313.

Mesinger, F., and A. Arakawa, 1976: Numerical methods used in atmospheric models. GARP Pub. Ser. No. 17, **1,** WMO-ICSU Joint Organizing Committee, 64 pp.

Montgomery, R. B., 1941: Transport of the Florida Current off Havana. *J. Mar. Res.,* **4,** 198–219.

Otterson, T., 1992: An analysis of the wind-forced response of Conception Bay using a reduced-gravity numerical model. M.S. thesis, Memorial University, St. John's, Newfoundland, 158 pp. [Available from Department of Physics, Memorial University, St. John's, Newfoundland, Canada, A1B 3X7.]

Rattray, M., 1982: A simple exact treatment of the baroclinicity–bathymetry interaction in a frictional, iterative, diagnostic ocean model. *J. Phys. Oceanogr.,* **12,** 997–1003.

Reid, J. L., and A. W. Mantyla, 1976: The effect of geostrophic flow upon coastal sea elevations in the northern North Pacific Ocean. *J. Geophys. Res.*, **81,** 3100–3110.

Sandström, J. W., and B. Helland-Hansen, 1903: Über die Berechnung von Meeresströmungen. Report on Norwegian fishery and marine investigations 2 (1902), Vol. 4, 43 pp.

Sarkisyan, A. S., and V. F. Ivanov, 1971: Joint effect of baroclinicity and bottom relief as an important factor in the dynamics of sea currents. *Izv. Acad. Sci. USSR, Atmos. Oceanic Phys.*, **7,** 173–188.

Schmitz, W. J., Jr., 1980: Weakly depth-dependent segments of the North Atlantic Circulation. *J. Mar. Res.*, **38,** 111–135.

Sverdrup, H. V., M. W. Johnson, and R. H. Fleming, 1942: *The Oceans: Their Physics, Chemistry and General Biology.* Prentice-Hall, 1060 pp.

Tabata, S., B. Thomas, and D. Ramsden, 1986: Annual and interannual variability of steric sea level along line P in the northeast Pacific Ocean. *J. Phys. Oceanogr.*, **16,** 1378–1398.

Tziperman, E., W. C. Thacker, R. B. Long, and S.-M. Hwang, 1992a: Oceanic data analysis using a general circulation model. Part I: Simulations. *J. Phys. Oceanogr.*, **22,** 1434–1457.

——, ——, ——, ——, and S. R. Rintoul, 1992b: Oceanic data analysis using a general circulation model. Part II: A North Atlantic Model. *J. Phys. Oceanogr.*, **23,** 1458–1459.